East European Journal of Physics. 4. 397-406 (2025)
DOI:10.26565/2312-4334-2025-4-38 ISSN 2312-4334

PHYSICAL PRINCIPLES OF PHOTOCURRENT GENERATION IN A SILICON-BASED PHOTODIODE STRUCTURE WITH A SCHOTTKY BARRIER

Feruza A. Giyasova[1], Akhmad Z. Rakhmatov[2], Khayot N. Bakhronov[3], Murodjon A. Yuldoshev[4]*, Farkhod A. Giyasov[1], Abdurauf N. Olimov[5], Nosirbek A. Sattarov[1]

[1]*Kimyo International University in Tashkent, Uzbekistan*
[2]*JSC Photon, Tashkent, Uzbekistan*
[3]*Tashkent University of Information Technologies named after Muhammad al-Khwarizmi, Uzbekistan*
[4]*Turan International University, Namangan, Uzbekistan*
[5]*Institute of Ion-Plasma and Laser Technologies, Uzbekistan Academy of Sciences, 33, Durmon Yuli St., 100125, Tashkent, Uzbekistan*
**Corresponding Author e-mail: murod.yuldoshev1993@gmail.com*
Received September 11, 2025; revised October 17, 2025; accepted October 29, 2025

Homojunction structures of the type Ag–nSi–n$^+$Si–(In+Sn) with perfect single-crystal (111) orientation and a high-resistivity compensated layer at the n$^+$Si/n-Si interface were obtained using the liquid-phase epitaxy method. The results of investigating photogeneration processes and current transport mechanisms in the silicon Schottky-barrier photodiode structure are presented. A two-barrier model of the structure was developed, according to which current transport has a multifactorial nature and is governed by the combined contributions of thermionic emission, tunneling, and generation–recombination processes. Furthermore, it was established that the photosensitivity of the studied structure covers a photon energy range of 0.387÷1.016 eV, shifted toward the long-wavelength region. The formation of a near-surface high-resistivity layer contributes to an increased response and enables photosensitivity values of up to 0.338 A/W. It was found that reducing the barrier capacitance to 8÷10 pF broadens the frequency range and enhances the speed of response. The Ag–nSi–n$^+$Si–(In+Sn) structures are promising for use in photodiodes of optoelectronic devices operating in the visible and infrared spectral regions.
Keywords: *Structure; Homojunction; Characteristic; Index; Mechanism; Capacity; Barrier; Photogeneration; Photosensitivity; Photocurrent; Intensity; Photodiode*
PACS: 64.70.kg, 73.40.Kp, 68.37.Hk

INTRODUCTION

At the current stage of information technology development, there is a need to create photodetectors with low noise levels, high stability, linear photoelectric characteristics, and minimal inertia [1–3]. The use of semiconductor structures in optoelectronic systems is driven by their inertial properties and the dependence of the photocurrent on both the applied voltage and the intensity of optical radiation [4]. Since optoelectronic systems operate at high frequencies, it is necessary to minimize signal delay in the photodetectors employed. Schottky-barrier diode structures are the most suitable for this purpose, as they offer the potential to reduce inertia by lowering capacitance [5].

For example, structures with two rectifying barriers [6] exhibit reduced capacitance compared to similar single-junction structures [7,8] and demonstrate superior performance under high-frequency operating conditions.

According to preliminary data [9], adding a second rectifying barrier to a potential-barrier structure helps to reduce its capacitance. However, the implementation of such a structure requires careful optimization of the base region parameters and precise control over the technology used to form the Schottky barriers. In addition, it is necessary to improve the noise characteristics, which depend not only on the magnitude of the reverse current but also on the operating mode of the device. From this standpoint, photodetectors operating in photovoltaic mode are of particular interest. Photovoltaic detectors belong to this class of semiconductor devices. Yet, they face a significant challenge: the surface layer of the p–n junction absorbs short-wavelength radiation, while long-wavelength radiation often passes through the junction without being absorbed.

These limitations can be overcome by creating multilayer heterojunction structures [10,11] with an extended spectral absorption range. Such structures are fabricated using molecular epitaxy, though certain technological constraints exist [12,13]. Noise reduction can be achieved by operating photodetectors in photovoltaic mode and by lowering the reverse dark currents. Additionally, the issue of inertia must be addressed. One of the most effective ways to overcome these issues is the development of advanced silicon-based Schottky-barrier photodetectors, which eliminate charge accumulation. The choice of silicon is justified by its extensive study and the well-established fabrication processes available for it. However, novel methods employed in gallium arsenide structures with metal–semiconductor junctions have not yet been applied to silicon systems. At the same time, further research is required to evaluate the potential outcomes.

It is known that in the early 1990s, research began on the physical and technological aspects of fabricating metal–semiconductor barrier structures based on silicon [14,15]. Photodetector structures were fabricated on bulk silicon, and

Cite as: F.A. Giyasova, A.Z. Rakhmatov, Kh.N. Bakhronov, M.A. Yuldoshev, F.A. Giyasov, A.N. Olimov, N.A. Sattarov, East Eur. J. Phys. 4, 397 (2025), https://doi.org/10.26565/2312-4334-2025-4-38

in some cases on epitaxial layers. Their spectral range depended on the material of the base region, with the maximum photocurrent observed near the intrinsic absorption wavelength (0.9÷1.0 μm) [16].

In conventional Schottky-barrier structures [17], the reverse currents exceed those typical of p–n junctions, which necessitates higher signal levels for their proper operation. To improve the photoelectric characteristics of silicon structures with double-sided barriers and to study the possible mechanisms of photosensitivity and their relationship to the parameters of the base region (such as thickness and carrier concentration), comprehensive physical and technological investigations are required. This includes developing new physical principles for the operation of such structures, which are promising for optoelectronic systems. This task remains relevant, as the challenge of creating low-noise photodetectors for optoelectronics has not yet been fully resolved.

At present, researchers are focused on the tasks of receiving and processing laser and optical radiation, paying particular attention to the development of suitable photodetectors [18]. Intensive efforts are being made to develop methods for creating photodetectors for the ultraviolet and infrared spectral ranges, where optical losses in fibers are minimal [19–21].

Elemental and binary semiconductors have begun to be used for their fabrication, where variation of the composition and thickness of the base region makes it possible to achieve photosensitivity over a wide spectral range (0.3÷1.8 μm) [22]. In particular, Schottky-barrier photodetectors based on silicon have been developed, in which charge carrier transport occurs primarily via thermionic emission [23,24]. It should be noted that the minimum detectable signal level turned out to be higher than in similar p–n junction structures. This is explained by the high saturation current (I_s) values resulting from the relatively low potential barrier height (φ). Functionally, Schottky-barrier and p–n junction structures are interchangeable. They are widely used for alternating-current rectification, as well as in mixer diodes, Zener diodes, pulse diodes, and parametric diodes [25–28]. Recently, new metal–thin dielectric–semiconductor (MIS) structures have emerged, providing semiconductor devices with a range of new functional properties [29].

In this regard, the present article examines the physical principles related to photogeneration processes in Schottky-barrier structures, which characterize the electronic phenomena occurring in the space-charge region of the potential barrier in the Ag–nSi–n^+Si–(In+Sn) photodiode structure. The structure under investigation is a complex multilayer metal–semiconductor–metal system, considered promising for use in photodiodes and sensor elements.

EXPERIMENTAL SAMPLES AND MEASUREMENT METHODS

The studies were performed using Ag-nSi-n^+Si-(In+Sn) homojunction photodiode structures formed on the basis of a heavily doped KEF-7.8 silicon substrate. The substrates were silicon wafers with a crystallographic orientation of (111), 25 mm in diameter and about 380 μm thick. The material was characterized by a carrier concentration of N_n=2.3×10 cm^{-3} and a resistivity of 7.8 Ohm cm. The wafers were made of single-crystal silicon provided by JSC Photon. The base region was a high-resistance silicon layer (ρ≈4.2×10^6 Ω·cm) 36 μm thick, characterized by n-type conductivity at a carrier concentration of N_n=1.1×10^9 $см^{-3}$.

The initial preparation of the silicon substrates consisted of grinding followed by double-sided polishing using ASM-1.5 diamond paste. Before applying the metal coatings, the silicon wafers were treated in a polishing etchant containing HF, HNO_3, and CH_3COOH in a 1:8:1 ratio. Afterward, they were thoroughly rinsed in deionized water and dried.

Next, an active n^+Si region was formed on the surface of the substrate -an epitaxial layer grown by liquid-phase epitaxy with a thickness of 36 μm. To reduce dark currents, the structures were annealed in a hydrogen flow at 310°C for 30 minutes.

As a contact layer, a silver (Ag) film was deposited on the surface of the active n-Si region, forming a potential barrier. The deposition was carried out in vacuum (~10^{-7} Torr) at 386°C from a silver source (mass 34 mg), resulting in a film thickness of 95 Å. On the back side of the structure, an ohmic contact was obtained by vacuum deposition of an (In+Sn) alloy (mass 53 mg) at 212 °C, with a thickness of 125 Å. The film thicknesses were measured using a Linnik MII-4 microinterferometer.

The resulting Ag-nSi-n^+Si-(In+Sn) homojunction structure was then scribed into discrete samples with an area of 5-9 mm^2. Structurally, the device is a semiconductor photodiode fabricated on a heavily doped substrate, as shown in Fig. 1.

Figure 1. Geometric cross-section of the single-base photodiode structure Ag-nSi-n^+Si-(In+Sn)

The current–voltage characteristics (I–V curves) of the Ag-nSi-n$^+$Si-(In+Sn) photodiode structure were recorded according to the standard circuit described in [30], in both forward and reverse bias, over a wide range of current and voltage values at room temperature (293 K). The operating voltage was supplied by B5-48 and B5-50 power supplies with a step of 0.05 V. Voltage and current were measured using universal voltmeters V7-21A and V7-35. The minimum measurable current was 2 nA, and the relative measurement error was 0.2÷0.4%.

The capacitance–voltage characteristics (C–V curves) of the structure were recorded over a wide frequency range from 50 Hz to 10 kHz. The study showed that in the frequency ranges f ≤ 100 Hz and f≥1 kHz, the C–V characteristics exhibit different features and capacitance values. Therefore, the primary focus of the investigation was on frequencies around 100 Hz and 8.3 kHz. The C–V characteristics of the studied homostructures were measured for capacitance values in the range C=1.0÷70 pF using the standard setup described in [30].

The illuminated current–voltage characteristics of the structure were measured under reverse current direction at room temperature (T=293 K) under illumination in the range E=0÷160 lx. Illumination of the structures was provided by a special incandescent lamp SIRSh 6-100 with power W=100 W, which is equivalent in its parameters to a standard white light reference lamp. It should be noted that one lumen of electromagnetic radiation in the visible spectral region corresponds to a power of $9.1 \cdot 10^{-3}$ W.

RESULTS AND DISCUSSION

The morphology of the Ag-nSi-n$^+$Si-(In+Sn) homostructure samples on silicon substrates was studied using a scanning electron microscope SEM EVO MA 10 (Carl Zeiss, Germany) and is shown in Fig. 2. For elemental composition analysis, an energy-dispersive X-ray spectrometer EDX (Oxford Instruments) – Aztec Energy Advanced X-act SDD – was used. During the measurements, an accelerating voltage of 15 kV was applied to the filament, with a working distance of 8.5 mm from the sample surface. Scanning was carried out from one side of the investigated homostructure.

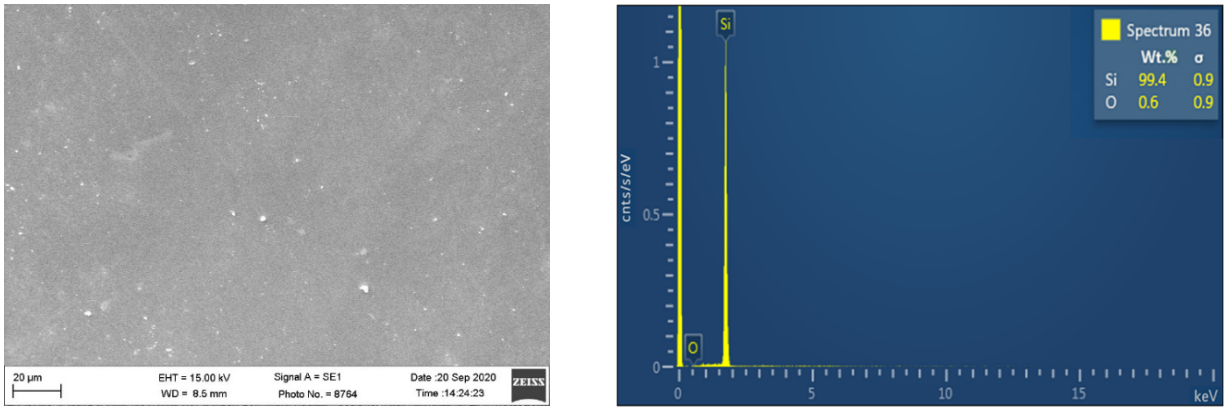

a b

Figure 2. SEM images of the surface (a) and elemental analysis (b) of the Ag-nSi-n$^+$Si-(In+Sn) homostructure based on n-type monocrystalline silicon

The data obtained using the scanning electron microscope (SEM) and presented in Fig. 2 indicate a dominant silicon content in the sample, which is confirmed by the high intensity of its main peak. The weak oxygen (O) peak suggests the possible presence of oxide compounds or surface contaminants formed during the growth or storage of the structure. According to the quantitative analysis, the mass fraction of silicon is 99.4%, while that of oxygen is 0.6%.

As is well known, such m-n-n$^+$-m structures are often used to study transient effects and rectification characteristics. The I–V characteristics of the Ag-nSi-n$^+$Si-(In+Sn) structure under forward and reverse bias, shown in linear (a) and semilogarithmic (b) scales, are presented in Fig. 3, in accordance with the equivalent circuit shown in Fig. 4.

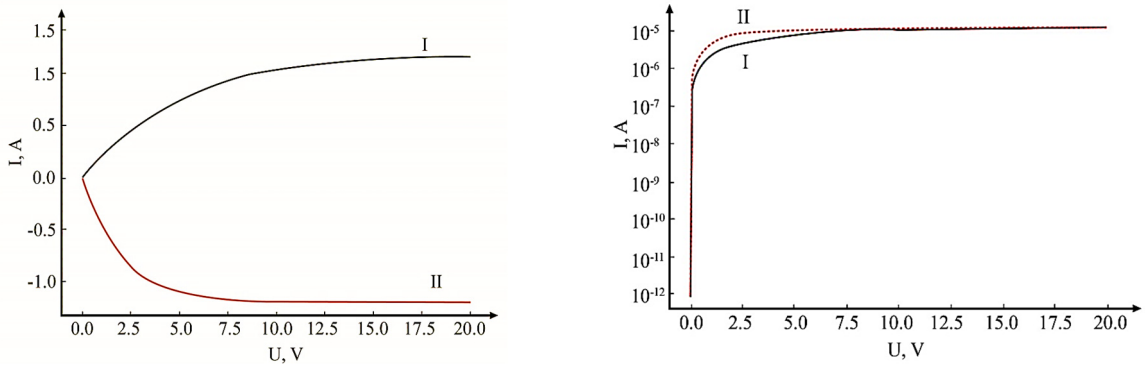

a b

Figure 3. Current–voltage characteristics of the Ag-nSi-n$^+$Si-(In+Sn) structure in linear scale (a) and semilogarithmic scale (b) under different biasing modes: I – (-) Ag-nSi-n$^+$Si-(In+Sn) (+), II – (+) Ag-nSi-n$^+$Si-(In+Sn) (-)

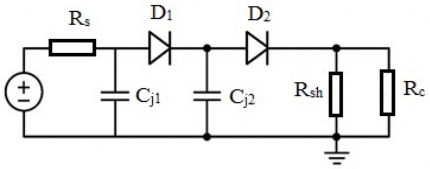

Figure 4. Two-barrier equivalent circuit of the Ag-nSi-n$^+$Si-(In+Sn) structure

Within the framework of the two-barrier approximation, the equivalent circuit of the structure can be represented as a series connection of two diodes (Fig. 4), which makes it possible to accurately describe the experimental current–voltage characteristics [31, 32]. This model includes the following elements:

- two oppositely connected diodes (D_1 and D_2) corresponding to the barriers $\varphi_{\beta 1}$ and $\varphi_{\beta 2}$: D_1 describes the Schottky barrier at the Ag–nSi contact, characterized by barrier height $\varphi_{\beta 1}$, series resistance R_s, saturation current I_{s1}, and junction capacitance C_{j1}; D_2 corresponds to the n–n$^+$Si junction, with similar parameters: $\varphi_{\beta 2}$, I_{s2}, and C_{j2}; series resistance R_s, taking into account ohmic losses in the volume of the semiconductor and contacts, expressed as,

$$R_s = R_{\text{contact}} + R_{\text{volumetric layer}} + R_{\text{substrates}}; \quad (1)$$

- parallel resistance R_{sh}, simulating leakage currents through defective channels and the periphery of the structure;
- barrier capacitances C_{j1} and C_{j2}, which determine the capacitive properties of the depleted regions.
- R_c is the resistance at the metal-semiconductor boundaries (Ag-nSi and (In+Sn)-n$^+$Si), caused by imperfect contacts and barrier effects, affecting the real current-voltage characteristic and photosensitivity of the structure.

The proposed two-barrier equivalent circuit is versatile, allowing a consistent interpretation of the experimental characteristics over a wide voltage range: from the low-voltage regime, where generation–recombination processes dominate, to the high-voltage region, where thermionic emission and tunneling through localized states become the determining mechanisms.

According to the equivalent circuit (Fig. 4), when the polarity of the applied voltage changes, the base is blocked alternately on one side or the other, which determines the current flowing through the structure [33]. The observed difference in the current values confirms that the Schottky barrier at the Ag-nSi contact and the isotypic n-n$^+$ junction (nSi-n$^+$Si with an (In+Sn) contact) have different electrical characteristics due to differences in the work function of the metals and the conditions for the formation of interphase boundaries. Under forward and reverse biases, the current is determined by a combination of charge carrier transport mechanisms, including thermionic emission through the Schottky barrier, tunneling current through the depletion layer, and recombination-generation processes in the space charge region [34]. An important factor is the change in the width of the depletion layer, which decreases under forward bias and expands under reverse bias, which directly affects the probability of tunneling and the effective barrier height. In addition, in real structures [33, 36], a significant role is played by localized states in the forbidden band of silicon, arising due to lattice defects and impurity centers. These states participate in recombination-generation processes and can significantly modify the shape of the I-V characteristic, especially in the region of low voltages. From the analysis of the I-V characteristic, it is evident that the dependence of the current on the voltage is approximated by a power function of the form $I \propto U^{\gamma}$ [37], with two characteristic sections being distinguished. In the forward bias region, the first section corresponds to the exponent $\gamma \approx 0.28$, which indicates a significant contribution of the tunneling mechanism through a narrow depletion layer. With a further increase in voltage, the exponent increases to $\gamma \approx 1.42$, which indicates a transition to the diffusion and thermionic transport mechanisms, consistent with a decrease in the effective barrier height [37]. The combined analysis of the current-voltage characteristics indicates the multifactorial nature of current transport, where the interaction of the barrier height plays a decisive role. The dynamics of the depletion layer width and localized states in the forbidden zone allow for a deeper interpretation of the conductivity mechanisms in the structure under study.

In the locking mode, the value of the power-law exponent in the initial section is ~1.15, which corresponds to an almost linear dependence of the current on the voltage $I \propto U^{\sim 1}$. This mode is interpreted as a manifestation of thermionic injection with insignificant nonlinearity and the absence of significant current limitation from the side of the barrier contact. In the next section, an increase in the power-law exponent to a value of about 2.84 is observed, which indicates a change in the dominant conductivity mechanism and the involvement of a volume-limited current with the participation of traps. It should be noted that in both cases, in the second characteristic measurement interval, the values of the power-law exponent approach 0.5. With forward bias, this indicates the impossibility of describing the structure behavior within the framework of the classical diode exponent; the current is formed due to defective conductivity channels. In the reverse bias mode, this indicator reflects the predominance of tunneling processes through the potential barrier, involving distributed localized states in the band gap associated with surface generation.

As follows from the equivalent circuit (Fig. 4), when a common external voltage $U_{general}^{(+)Ag-nSi-n+Si-(In+Sn)(-)}$ is applied to the structure, a total current will flow:

$$U_{general}^{(+)Ag-nSi-n+Si-(In+Sn)(-)} = U_{straight}^{(+)Ag-nSi} = U_{arr}^{n+Si-(In+Sn)} \quad (2)$$

However, the total voltage consists of the sum of the voltages dropped at each junction:

$$U_{general}^{(+)Ag-nSi-n+Si-(In+Sn)(-)} = U_{1straight}^{(+)Ag-nSi} + U_2^{nSi-n+Si} + U_{3arr}^{n+Si-(In+Sn)} \quad (3)$$

The potential barrier height for the Ag-nSi transition is 0.65 eV, and for the isotypic nSi-n$^+$Si transition it is 0.197 eV. Using data on the carrier concentration and the effective density of states in the conduction band of silicon ($N_c \approx 2\times1018$ cm^{-3}), the position of the Fermi level was calculated using the formula [37]:

$$Å_F = E_C - \frac{kT}{q}\ln\left(\frac{N_C}{N_D}\right) \quad (4)$$

which was found to be 0.622 eV relative to the conduction band edge. It should be noted that this Fermi level value indicates a pronounced degree of semiconductor degeneracy, in which the carrier distribution deviates from the classical Maxwellian distribution and must be described using Fermi–Dirac statistics [38]. Such a shift of the Fermi level has a direct effect on the depletion layer width in the junction: at high impurity concentrations, the depletion layer becomes significantly narrower, which increases the probability of tunneling through the barrier and changes the dominant current transport mechanisms. Thus, the obtained parameters of the barrier height and Fermi level are consistent with the features of transport processes in multilayer metal–semiconductor structures and isotype heterojunctions. Accordingly, the difference between the conduction band edge and the Fermi level is 0.59 eV, and the difference between the barrier height and this value gives the contact potential differences for the junctions:

U_c^{Ag-nSi}= - 0.412 eV, $U_c^{nSi-n+Si}$= 0.554 eV, $U_c^{n+Si-(In+Sn)}$= 0.152 eV. The potential difference between the Ag-nSi and n$^+$Si-(In+Sn) junctions is 0.625 eV.

Assuming an abrupt metal–semiconductor junction, the corresponding widths of the space-charge regions ($W^{m_1-n}$and W^{n-m_2}) can be determined based on the formula [37]:

$$W^{m-n} = \left[\frac{2\varepsilon\varepsilon_0}{qN_D}(U_C \pm U_{adj})\right]^{1/2} \quad (5)$$

In the absence of an external bias, the initial thicknesses of the space-charge regions formed by the rectifying barriers were calculated. The obtained values were $W_0^{m_1-n}$ =672.8 μm and $W_0^{n-m_2}$=5.49 nm, which reflects a significant contrast in the spatial distribution of the electric field at different junctions. Using the method for determining the voltage drop across each junction [39], based on the experimental I–V characteristics, the values of U_1^{Ag-nSi}, $U_2^{n+Si-nSi}$ and $U_3^{n+Si-(In+Sn)}$, were obtained, as well as the thicknesses of the space-charge layers of each junction, which are presented in Table 1.

Table 1. Calculated data of physical parameters at transitions

(-)Ag-nSi-n$^+$Si-(In-Sn)(+)								
$U_{general}$ (V)	$I_{general}$ (μA)	U_1 (V)	U_2 (V)	U_3 (V)	E (V/см)	W_1(μm)	W_2(μm)	W_3(μm)
0.1	0.06	0	0.705	0.320	5.55	254.3	675.2	0.0037
0.5	0.37	0.106	1.125	0.712	27.74	568.6	845.3	0.0056
1.0	0.64	0.615	1.605	1.218	55.49	804.1	1018.7	0.0073
1.5	0.92	1.117	2.132	1.672	83.23	984.8	1166.6	0.0086
2.0	1.23	1.504	2.412	2.185	110.97	1137.2	1297.8	0.0098
2.5	1.57	2.119	3.113	2.720	138.72	1272.7	1417.6	0.0110
3.0	1.82	2.606	3.515	3.136	166.46	1395.4	1529.3	0.0121
3.5	2.11	3.107	4.088	3.697	194.20	1507.9	1636.0	0.0132
4.0	2.45	3.616	4.565	4.210	221.94	1612.8	1739.3	0.0143
4.5	2.73	4.099	5.133	4.703	249.69	1711.9	1840.2	0.0154
5.0	3.16	4.428	5.497	5.301	277.43	1806.6	1939.6	0.0165
10.0	6.78	9.701	10.605	9.327	554.86	2538.8	3089.0	0.0231
15.0	9.12	14.596	16.212	15.583	832.29	3114.3	3186.1	0.0290
20.0	12.0	19.606	21.101	20.158	1109.72	3577.7	3484.6	0.0346

Table 1 also shows the values of the maximum electric field strength in the turn-off junctions. It is important to note that the dependence of the current calculated relative to the falling voltage completely reproduces the course of the curve on the total turn-off voltage (Fig. 3), which indicates the identity of the current transfer mechanisms. As follows from the data in Fig. 3, in forward-biased junctions the current increases linearly with increasing falling voltage; the exponent $\gamma \sim 1$, corresponds to the thermionic emission mode. In this case, the applied voltage in the forward-biased junction cannot exceed the value of the contact potential difference, as a result of which its main part is distributed over the quasi-neutral region of the base r_{bases}, that is, $U_{straight}^{Ag-nSi} = U_{straight}^{Ag-nSi^*} + U_{r_{bases}}$, connected in

series with the junction. Such voltage redistribution directly affects the width of the depletion layer, decreasing it with increasing forward bias, which, in turn, facilitates the injection of carriers through the barrier and leads to a change in the current transfer conditions [40].

Based on the equivalent circuit (Fig. 4) describing the two-barrier model of the Ag–nSi–n$^+$Si–(In+Sn) structure, the following features of the current transport mechanism can be distinguished:

- in the low-voltage region (|U|<0.3 V), the current is dominated by generation–recombination through the barrier φ_{v1} in the depletion region, which is reflected in its quasi-linear increase;
- at medium voltages (0.3÷1 V), the main mechanism becomes thermionic emission through the φ_{v1} barrier, which is characterized by an exponential dependence of the current on the applied voltage;
- in the region of high voltages (U>1÷2 V) the second barrier φ_{v2} is activated, tunneling processes with the participation of localized states are enhanced, which leads to a power dependence of the type $I \sim U^{\gamma}$ with fractional values of the exponent γ.

The measurements of the VEH were carried out in the voltage range from -15 V to +15 V. The dependences of the capacitance C(U) were recorded (Fig. 5), which were then recalculated into coordinates C^{-2} (U) [37]. The dependence of the capacitance on the voltage in coordinates C^{-2}~U (Fig. 6) in the initial section gives a straight line, confirming the sharpness of the p-n junction.

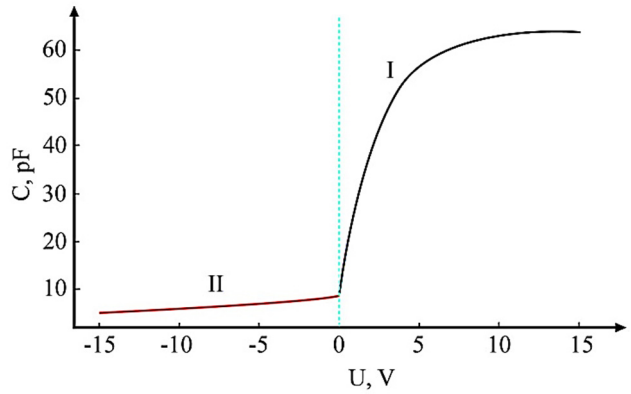

Figure 5. Volt-capacitive characteristic of the Ag-nSi-n$^+$Si-(In+Sn) structure under forward (I) and reverse (II) bias

Fig. 5 shows the VEC of the studied Ag-nSi-n$^+$Si-(In+Sn) structure. The experimental data show two characteristic modes of capacitance behavior depending on the magnitude of the applied voltage. In the region of reverse voltages (0…−15 V), a monotonic decrease in capacitance from ~9 pF to ~5 pF is observed. This effect is due to the expansion of the depletion layer and corresponds to the barrier capacitance of the p-n junction, which is described by the expression [34,37]:

$$C_{bar} \cong S\sqrt{\frac{q\varepsilon\varepsilon_o N}{2(\phi_{con}-U)}}, \tag{6}$$

where, N is the impurity concentration in the lightly doped region, S is the area of the structure, U is the blocking voltage, ϕ is the height of the metal-semiconductor barrier.

Therefore, as the reverse bias modulus increases, the width of the depletion layer increases, which leads to a decrease in the barrier capacitance.

When moving to the region of forward biases (0…+15 V), an exponential growth of capacitance is observed, reaching ~64 pF at +15 V. This effect is due to the dominance of the diffusion component associated with the injection and accumulation of charge carriers near the junction. The diffusion capacitance is described by the dependence [34]:

$$C_d \propto \exp(qV/kT), \tag{7}$$

Thus, the analysis of the VEH shows that in the region of reverse voltages, the main mechanism of capacitance change is the redistribution of the space charge and the expansion of the depletion layer, whereas in the region of forward bias, the process of diffusion injection dominates.

Fig. 6 shows the dependence C^{-2} (U) for the studied structure; linear approximation in the reverse bias region allowed us to determine key parameters such as: charge carrier concentration, depletion layer width, and potential barrier height of the junction. In particular, the value of the built-in potential was $\varphi_v \approx 0.185$ V, and the concentration of donor impurities was $N_D \approx 5.2\times1011$ cm^{-3}. The analysis technique is based on the Mott-Schottky equation, which relates the capacitance of the barrier junction to the applied voltage [34, 37]:

$$C^{-2} = (2/q\varepsilon\varepsilon_0 N_D S^2) \cdot (\varphi_v - U), \tag{8}$$

where, q is the electron charge, ε is the relative permittivity of silicon, ε_0 is the electric constant, S is the area of the structure, U is the external voltage, and φ_v is the built-in potential.

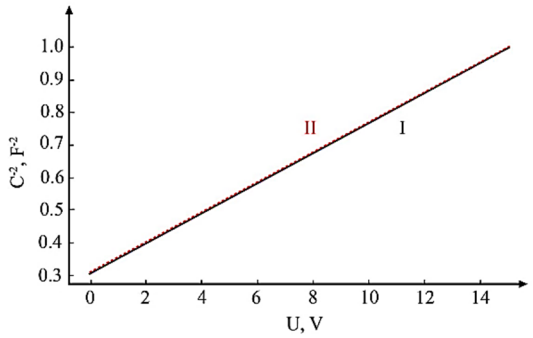

Figure 6. Dependence C^{-2} (U) by the Mott-Schottky method for the Ag–nSi–n^+Si–(In+Sn) structure with superimposed linear approximation

The linear section of the C^{-2} (U) graph indicates a uniform distribution of impurities in the semiconductor volume. The donor concentration N_D is determined from the slope of the straight line, and the intersection point with the voltage axis yields the value of φ_{con}. Optimization of the parameters of the base silicon region (thickness ≈36 μm and specific resistance 4.2×106 Ω·cm) leads to a decrease in the concentration of charge carriers and, as a consequence, a decrease in the barrier capacitance of the structure to 8÷10 pF, which is almost an order of magnitude less compared to 70÷110 pF for photodiodes based on GaAsSb solid solutions for the IR region, providing a twofold expansion of the operating frequency range and an increase in response time, which gives the structure under consideration a significant advantage over analogs based on gallium arsenide and antimony compounds [41, 42].

The dependences of the photocurrent on the operating voltage during excitation from the Ag-nSi junction side by integrated light with a maximum at λ=0.55 μm of the Ag-nSi-n^+Si-(In+Sn) structure in the potential barrier locking mode under different illuminations are shown in Fig. 7 [43].

Figure 7. Illuminated current–voltage characteristics of the Ag–nSi–n^+Si–(In+Sn) structure in the reverse-bias mode: 1 – 0 lx, 2 – 100 lx, 3 – 200 lx, 4 – 1000 lx, 5 – 2000 lx

As can be seen from Fig. 7, in darkness the current–voltage dependence is nearly linear. Under the action of broadband light from a tungsten lamp with a spectral maximum near 0.86 μm, an increase in photocurrent is observed with increasing reverse bias voltage up to 2 V and illumination intensity, indicating a higher photocurrent compared to its initial value at 0.02 V. The optimal operating voltage range is 0.8÷1.2 V.

The dependence of the response sensitivity on wavelength (Fig. 8) qualitatively corresponds to the characteristic curve of a silicon photodiode with a p–n junction, and the spectral sensitivity range extends from 0.48 to 1.26 μm.

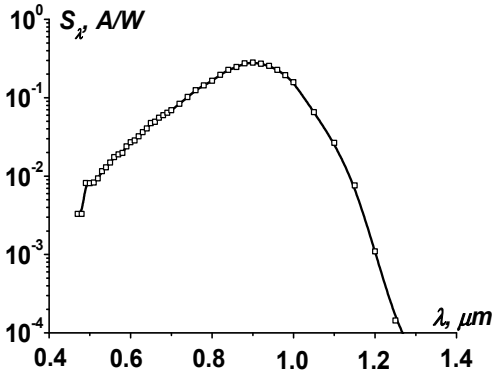

Figure 8. Wavelength dependence of the response sensitivity of the Ag–nSi–n^+Si–(In+Sn) structure

The spectral optical range of the Ag–nSi–n^+Si–(In+Sn) structure is relatively broad, extending from λ=0.48 to 1.26 μm, with a maximum response at 0.92 μm. This behavior is explained by the presence of a thin, high-resistivity layer located near the surface. The spectral range extends into the near-infrared region due to deep impurity levels positioned near the mid-gap in the subsurface region of silicon, which become ionized under reverse bias. As the operating voltage increases from 0.02 V to 2.0 V, the photocurrent rises correspondingly, particularly in the range of λ=0.9÷1.25 μm. The formation of an active near-surface layer with increased resistivity leads to enhanced photosensitivity across the investigated spectral range, reaching a value of 0.338 A/W [33, 44]. The spectral photocurrent exhibits a monotonic increase with applied voltage, which is attributed to the higher rate of photogenerated carriers in the space-charge region controlled by the Ag–nSi junction [45,46].

CONCLUSIONS

The homojunction structures Ag–nSi–n^+Si–(In+Sn), obtained by the liquid-phase epitaxy method, exhibit a perfect single-crystalline film with (111) orientation and subcrystallite sizes exceeding 50 nm [47]. During the liquid-phase epitaxy of the solid solution, a compensated high-resistivity layer is formed at the interface between the n^+-Si substrate and the n-Si epitaxial film, characterized by a resistivity of 3.2×10^4 Ω·cm at room temperature (293 K).

The analysis of the I–V characteristics of the Ag–nSi–n^+Si–(In+Sn) structure revealed that charge transport is multifactorial, determined by thermionic emission, tunneling, and generation–recombination processes. A significant influence is exerted by the differences in the electrical characteristics of the Schottky barrier and the isotype junction, the dynamics of the depletion layer width, as well as localized states caused by defects and impurity centers. The power-law behavior of the current–voltage dependence indicates a change in the dominant conduction mechanisms under different bias regimes: from tunneling transport at low voltages to diffusion–thermionic and trap-assisted space-charge-limited current at higher voltages [48]. The photosensitivity of the studied structure covers a spectral photon energy range of 0.387÷1.016 eV, being shifted toward the long-wavelength region compared to conventional pSi–nSi silicon structures; additional formation of a high-resistivity near-surface layer enhances the response, allowing photosensitivity to reach 0.338 A/W. The maximum photocurrent increase at $E_{ph}\approx0.74$ eV indicates the generation of nonequilibrium minority carriers (holes) in the electronic transitions. It should be emphasized that the highest photocurrent value in the impurity absorption region is achieved under the condition that the thermal generation rate of electrons from silicon impurity levels is comparable to the rate of photogeneration of minority carriers via electron transitions from the valence band to these levels [49]. Optimization of the parameters of the silicon base region ensures a reduction in barrier capacitance down to 8÷10 pF, which is almost an order of magnitude lower than that of GaAsSb photodiodes (70÷110 pF), thereby enabling an extended operating frequency range and improved response speed.

Ag–nSi–n^+Si–(In+Sn) structures show potential for use as photodiodes in optoelectronic devices operating in the visible and infrared spectral regions. The results presented here can be applied to improve the photoelectric properties of silicon photodiode systems with metal–semiconductor junctions.

ORCID

Feruza A. Giyasova, https://orcid.org/0000-0003-0746-4986; **Murodjon A. Yuldoshev,** https://orcid.org/0000-0002-9722-9439
Khayot N. Bakhronov, https://orcid.org/0009-0000-4138-3149; **Farkhod A. Giyasov,** https://orcid.org/0009-0003-9882-0655
Nosirbek A. Sattarov, https://orcid.org/0009-0005-0506-0269

REFERENCES

[1] J. Davila-Rodriguez, X. Xie, J. Zang, C. J. Long, T. M. Fortier, H. Leopardi, T. Nakamura, J. C. Campbell, S.A. Diddams, F. Quinlan, "Optimizing the linearity in high-speed photodiodes," Instrumentation and Detectors, arXiv.1808.04429, (2018). https://doi.org/10.48550/arXiv.1808.04429
[2] T. Kauten, B. Pressl, T. Kaufmann, and G. Weihs, "Measurement and modeling of the nonlinearity of photovoltaic and Geiger-mode photodiode," Rev. Sci. Instrum. **85**, 063102 (2014). https://doi.org/10.1063/1.4879820
[3] C.A.R. Perini, G. Ferrari, J.-P. Correa-Baena, A. Petrozza and M. Caironi, "A solution processed metal oxide:polymer interlayer improves the perovskite photodetector response speed, dark current, and stability," The Royal Society of Chemistry's, EES Solar (2025). https://doi.org/1039/D5EL00043B
[4] Q. Zhao, W. Wang, F. Carrascoso-Plana, W. Jie, and T. Wang, A. Castellanos-Gomez, and R. Frisenda, "The role of traps in the photocurrent generation mechanism in thin InSe photodetectors," Materials Horizons, **7**, 252 (2020). https://doi.org/10.1039/C9MH01020C
[5] Q. Chen, X. Zhang, M.S. Sharawi, and R. Kashya, "Advances in High -Speed, High–Power Photodiodes: From Fundamentals to Applications," Appl. Sci. **14**, 3410 (2024). https://doi.org/10.3390/app14083410
[6] O.A. Abdulkhaev, G.O. Asanova, D.M. Yodgorova, and A.V. Karimov, "Investigation of the photoelectric characteristics of photodiode structures with silicon-based potential barriers," Journal of Engineering Physics and Thermophysics, **85**(3), 709-715 (2012). https://doi.org/10.1007/s10891-012-0705-y
[7] M. Casalino, G. Coppola, M. Iodice, I. Rendina, and L. Sirleto, "Near-Infrared Sub-Bandgap All-Silicon Photodetectors: State of the Art and Perspectives," Sensors, **10**, 10571-10600 (2010). https://doi.org/10.3390/s101210571
[8] O. Surucu, D.E. Yıldız, and M. Yıldırım, "A study on the dark and illuminated operation of Al/Si3N4/p Si Schottky photodiodes: optoelectronic insights," Applied Physics A, **130**, 103 (2024). https://doi.org/10.1007/s00339-024-07284-2
[9] S. Khudaverdyan, A. Vaseashta, G. Ayvazyan, L. Matevosya, A. Khudaverdyan, M. Khachatryan, and E. Makaryan, "On the Selective Spectral Sensitivity of Oppositely Placed Double-Barrier Structures," Photonics, **9**, 558 (2022). https://doi.org/10.3390/photonics9080558

[10] X. Guan, *et al*., "Recent progress in short- to long-wave infrared photodetection using 2D materials and heterostructures," Advanced Optical Materials, **9**(4), 1-24 (2021). https://doi.org/10.1002/adom.202001708
[11] A. Bablich, *et al*., "Few-Layer MoS_2/a-Si:H Heterojunction Pin-Photodiodes for Extended Infrared Detection," ACS Photonics, **6**, 1372-1378 (2019). https://doi.org/10.48550/arXiv.1907.09592
[12] V.S. Varavin, S.A. Dvoretskii, N.N. Mikhailov, V.G. Remesnik, I.V. Sabinina, Yu.G. Sidorov, V.A. Shvets, *et al*., "Molecular Beam Epitaxy of CdHgTe: Current State and Horizons," Optoelectronics, Instrumentation and Data Processing, **56**(5), 456-469 (2021). https://doi.org/10.3103/S8756699020050143
[13] I. Izhnin, A. Izhnin, H. Savytskyy, O. Fitsych, N. Mikhailov, V. Varavin, S. Dvoretsky, *et al*., "Defects in HgCdTe grown by molecular beam epitaxy on GaAs substrates," Opto-electronics review, **20**(4), 375-378 (2012). https://doi.org/10.2478/s11772-012-0048-4
[14] M. Wittmer, "Carrier recombination and high barrier Schottky diodes on silicon," Solids and Materials, **51**, 451–454 (1990). https://doi.org/10.1007/BF00324725
[15] M Wittmer, and J.L. Freeouf, "Ideal Schottky diodes on passivated silicon," Phys. Rev. Lett. **69**(18), 2701-2704 (1992). https://doi.org/10.1103/PhysRevLett.69.2701
[16] T. Saito, "Spectral Properties of Semiconductor Photodiodes," in: *Advances in Photodiodes*, edited by G.-F.D. Betta, (IntechOpen, London, 2011), pp. 1-24. https://doi.org/10.5772/15300
[17] P. Pipinys, A. Pipiniene, and A. Rimeika, "Phonon-assisted tunneling in reverse biased Schottky diodes," J. Appl. Phys. **86**, 6875-6878 (1999). https://doi.org/10.1063/1.371766
[18] Z. Li, X. Jin, C. Yuan, and K. Wang, "Photon Detector Technology for Laser Ranging: A Review of Recent Developments," Coatings, **15**, 798 (2025). https://doi.org/10.3390/coatings15070798
[19] D. Ma, Y. Wang, and Y. Wang, "Performance enhancement of fiber-optic ultraviolet photodetector based on Ag/ZnO-microrod Schottky junction," in: *Proc. SPIE 12617, Ninth Symposium on Novel Photoelectronic Detection Technology and Applications (NDTA 2022)*, vol. 126175D, (2023). https://doi.org/10.1117/12.2666501
[20] Y.-F. Xiong, J.-H. Chen, Y.-Q. Lu, and F. Xu, "Optical-Fiber-Compatible Photodetector Based on a Graphene-MoS_2-WS_2 Heterostructure with a Synergetic Photogenerating Mechanism," Advanced-Electronic-Materials, **5**(1), 1800562 (2018). https://doi.org/10.1002/aelm.201800562
[21] S. Rakhmanov, K. Matchonov, H. Yusupov, K. Nasriddinov, and D. Matrasulov, "Optical high harmonic generation in Dirac materials," Eur. Phys. J. B, **98**, 35 (2025). https://doi.org/10.1140/epjb/s10051-025-00885-7
[22] M. Wang, *et al*., "Silicon-Based Intermediate-Band Infrared Photodetector Realized by Te Hyperdoping," Adv. Optical Mater. **9**, 2101798 (2021). https://doi.org/10.1002/adom.202101798
[23] Y. Jin, J. Seok, and K. Yu, "Highly Efficient Silicon-Based Thin-Film Schottky Barrier Photodetectors," ACS Photonics, **10**(5), 1-2 (2023). https://doi.org/10.1021/acsphotonics.2c01923
[24] A. Pelella, A. Grillo, E. Faella, G. Luongo, M.B. Askari, and A. Di Bartolomeo, "Graphene–Silicon Device for Visible and Infrared Photodetection," ACS Appl. Mater. **13**, 47895-47903 (2021). https://doi.org/10.1021/acsami.1c12050
[25] R. Aly, R. Tarek, O. Ramadan, and M. Khashan, "An Overview on Schottky Barrier Diodes," Faculty of Engineering-Alexandria University, 1-10 (2025). https://www.researchgate.net/publication/366763152
[26] B. Zhang, D. Ji, Y. Min, Y. Fan, and X. Chen, "A High-Efficiency 220 GHz Doubler Based on the Planar Schottky Varactor Diode," J. Electron. Mater. **48**, 3603–3611 (2019). https://doi.org/10.1007/s11664-019-07067-z
[27] M. Alathbah, "Development and Modelling of Gallium Nitride Based Lateral Schottky Barrier Diodes with Anode Recesses for mm Wave and THz Applications," Micromachines, **14**(2), 2-18 (2023). https://doi.org/10.3390/mi14010002
[28] C.-C. Hsieh, Y.-F. Chang, Y.-C. Chen, H.-L. Chang, and S.K. Banerjee, "Highly Non linear and Reliable Amorphous Silicon Based Back to Back Schottky Diode as Selector Device for RRAM Arrays," ECS Journal of Solid State Science and Technology, **6**(9), 143-147 (2017). https://doi.org/10.1149/2.0041709jss
[29] H. Chouaib, M. Aouassa, and M. Bouabdellaoui, "Highly photosensitive MIS structure with embedded silicon film for solar cell and photodetection applications," Journal of Materials Science: Materials in Electronics, **34**, 1815 (2023). https://doi.org/10.1007/s10854-023-11171-6
[30] F.A. Giyasova, "Development of Multilayer Photosensitive Structures Based on GaAs and Si for Optoelectronic Devices," D.Sci. thesis, Institute of Semiconductor Physics and Microelectronics, Uzbekistan (2024).
[31] A. Grillo, and A. Di Bartolomeo, "A Current-Voltage Model for Double Schottky Barrier Devices," Advanced Electronic Materials, **7**, 2000979 (2021). https://doi.org/10.1002/aelm.202000979
[32] N.N. Kononov, and S.G. Dorofeev, "Characteristics of the Schottky barriers of two-terminal thin-film Al/nano-Si film/ITO structures," Semiconductors, **51**, 608–616 (2017). https://doi.org/10.1134/S106378261705013X
[33] Sh. B. Utamuradova, F.A. Giyasova, M.S. Paizullakhanov, S.Yu. Gerasimenko, M.A. Yuldoshev, S.R. Boydedayev, and M.R. Bekchanova, "Investigation of the functional capability of modified silicon-based photodiodes structure," Chalcogenide Letters. **22**(8), 753-764 (2025). https://doi.org/10.15251/CL.2025.228.753
[34] A.G. Milnes, and D.L. Feucht, "Heterojunctions and Metal-Semiconductor Junctions," (Elsevier Science Imprint, 2012).
[35] V. Kumar, R. Singh, and P.K. Basu, "Current transport mechanisms in metal–semiconductor contacts," J. Appl. Phys. **110**(2), 024502-1–024502-7 (2011).
[36] R. Singh, and S. Kumar, "Trap-assisted space-charge-limited conduction in semiconductor structures," Solid-State Electronics, **45**(4), 625-630 (2001).
[37] S.M. Sze, and K.K. Ng, *Physics of Semiconductor Devices*, 3rd ed, (Wiley, Hoboken, NJ, USA, 2007).
[38] J.R. Yusupov, M. Ehrhardt, Kh.Sh. Matyokubov, and D.U. Matrasulov, "Driven transparent quantum graphs," Physica Scripta, **100**(7), (2025). https://doi.org/10.1088/1402-4896/ade014
[39] A.V. Karimov, and D.M. Yodgorova, "Determination of characteristics of double-barrier photodiode structures with metal-semiconductor junctions," Technology and design in electronic equipment, (5), 27-30 (2005). (in Ukrainian)
[40] D.M. Yodgorova, A.V. Karimov, F.A. Giyasova, R.A. Saidova, A.A. Yakubov, "Spectral photosensitivity m-n -n of structure on a basis epitaxy of layers," Semiconductor Physics Quantum Electronics Optoelectronics, **11**(1), 26-28 (2008). https://doi.org/10.15407/spqeo11.01.026

[41] E.V. Kunitsyna, I.A. Andreev, G.G. Konovalov, E.V. Ivanov, A.A. Pivovarova, N.D. Il'inskaya, and Yu.P. Yakovlev, "GaSb/GaAlAsSb Heterostructure Photodiodes for the Near-IR Spectral Range," Semiconductors, **52**, 1215-1220 (2018). https://doi.org/10.1134/S1063782618090099
[42] Sh.B. Utamuradova, F.A. Giyasova, K.N. Bakhronov, M.A. Yuldoshev, M.R. Bekchanova, B. Ismatov. Current Transfer Mechanism in A Thin-Based Heterosystem Based on A^2B^6 Compounds. East Eur. J. Phys. (2025), **3**, 325. https://doi.org/10.26565/2312-4334-2025-3-31
[43] D.M. Yodgorova, and F.A. Giyasova, "Photoelectric characteristics of silicon n^+-nSi-Ag structure," International Conference "Fundamental and Applied Issues of Physics". Section II: Physics of Semiconductors and Solids, Their Applied Aspects, **13-14**, 137-139 (2017).
[44] M.A. Yuldoshev, Z.T. Azamatov, A.B. Bakhromov, M.R. Bekchanova, East Eur. J. Phys. (4), 250 (2024), https://doi.org/10.26565/2312-4334-2024-4-25
[45] M. Akramov, B. Eshchanov, S. Usanov, Sh. Norbekov, and D. Matrasulov, "Second-harmonic generation in branched optical waveguides: Metric graphs based approach," Physics Letters A, **524**, 129827 (2024), doi.org/10.1016/j.physleta.2024.129827
[46] F.A. Giyasova, and M.A. Yuldoshev, "Investigation of temporal characteristics of photosensitive heterostructures based on gallium arsenide and silicon," Chalcogenide Letters, 22(2), 123–129 (2025). https://doi.org/10.15251/CL.2025.222.123
[47] A.S. Saidov, Sh.N. Usmonov, M.U. Kalanov, A.N. Kurmantayev, and A.N. Bahtybayev, "Structural and Some Electrophysical Properties of the Solid Solutions Si1–xSnx (0≤x≤0.04)," Phys. Solid State, **55**, 45-53 (2013). https://doi.org/10.1134/S1063783413010290
[48] A.V. Karimov, D.M. Yodgorova, F.A. Giyasova, E.M. Shpilevskiy, and N.I. Usmanova, "Photovoltaic Effect in Au-nSi-Au Structures with Schottky Barriers and Features of Spectral Characteristics," Applied Solar Energy, **54**(5), 330-332 (2018). https://doi.org/10.3103/S0003701X18050109
[49] A.S. Saidov, Sh.N. Usmonov, M. Kalanov, and Kh.M. Madaminov, "Structure and Photoelectric Properties of $Si_{1-x}Sn_x$ Epilayers," Tech. Phys. Lett. **36**, 827–829 (2010). https://doi.org/10.1134/S1063785010090154

ФІЗИЧНІ ПРИНЦИПИ ГЕНЕРАЦІЇ ФОТОСТРУМУ В КРЕМНІЄВІЙ ФОТОДІОДНІЙ СТРУКТУРІ З БАР'ЄРОМ ШОТТКІ

Ф.А. Гіясова[1], А.З. Рахматов[2], Х.Н. Бахронов[3], М.А. Юлдошев[4], Ф.А. Гіясов[1], А.Н. Олімов[5], Н.А. Саттаров[1]
[1]Міжнародний університет Кімьо в Ташкенті, Узбекистан
[2]ВАТ «Фотон», Ташкент, Узбекистан
[3]Ташкентський університет інформаційних технологій імені Мухаммада аль-Хорезмі, Узбекистан
[4]Міжнародний університет Туран, Наманган, Узбекистан
[5]Інститут іонно-плазмових та лазерних технологій Академії наук Узбекистану, вул. Дурмон Юлі, 33, 100125, Ташкент, Узбекистан

Гомоперехідні структури типу Ag–nSi–n^+Si–(In+Sn) з ідеальною монокристалічною (111) орієнтацією та шаром з високим опором, компенсованим на межі розділу n^+Si/n-Si, були отримані методом рідкофазної епітаксії. Представлено результати дослідження процесів фотогенерації та механізмів струмопереносу в кремнієвій фотодіодній структурі з бар'єром Шотткі. Було розроблено двобар'єрну модель структури, згідно з якою струмоперенос має багатофакторну природу та визначається комбінованим внеском термоелектронної емісії, тунелювання та процесів генерації-рекомбінації. Крім того, було встановлено, що фоточутливість досліджуваної структури охоплює діапазон енергій фотонів 0,387÷1,016 еВ, зміщений у довгохвильову область. Формування приповерхневого шару з високим опором сприяє підвищенню відгуку та дозволяє досягти значень фоточутливості до 0,338 А/Вт. Було виявлено, що зменшення бар'єрної ємності до 8÷10 пФ розширює діапазон частот та підвищує швидкість відгуку. Структури Ag–nSi–n^+Si–(In+Sn) є перспективними для використання у фотодіодах оптоелектронних пристроїв, що працюють у видимому та інфрачервоному діапазонах спектра.

Ключові слова: *структура; гомоперехід; характеристика; індекс; механізм; ємність; бар'єр; фотогенерація; фоточутливість; фотострум; інтенсивність; фотодіод*